Cancer Chemotherapy and Pharmacology (2019) 84:1187–1194
https://doi.org/10.1007/s00280-019-03953-9

ORIGINAL ARTICLE

Enhancing intratumoral biodistribution and antitumor activity of nab-paclitaxel through combination with a vascular disrupting agent, combretastatin A-4-phosphate

Meng Gao[1,2,3] · Dongjian Zhang[2,3] · Nan Yao[2,3] · Qiaomei Jin[2,3] · Cuihua Jiang[2,3] · Jian Zhang[2,3] · Feng Wang[4]

Received: 6 May 2019 / Accepted: 21 August 2019 / Published online: 13 September 2019

Abstract

Nanomedicines can generally only reach cancer cells at the edges of tumors, leaving most tumor cells in the central regions untreated. Previous studies showed that treatment with the vascular disrupting agent combretastatin-A4-phosphate (CA4P) can disrupt tumor vasculature, causing vascular shutdown and leading to massive necrosis in the tumor core. In this research, we explored the effect of co-administration of CA4P on the antitumor activity of nanoparticle albumin-bound paclitaxel (nab-paclitaxel) in Walker 256 tumor-bearing rats. The iodine 131 isotope was used for tracing and biodistribution analysis of nab-paclitaxel uptake. Liquid chromatography coupled with tandem mass spectrometry was performed to detect the intratumoral concentration of paclitaxel. Magnetic resonance imaging (MRI) was used to evaluate the effect of tumor treatment. Biodistribution results demonstrated that the tumor accumulations of both nab-paclitaxel and paclitaxel in the ^{131}I-nab-paclitaxel + CA4P group were much higher than those in the ^{131}I-nab-paclitaxel group. Nab-paclitaxel in combination with CA4P inhibited tumor growth significantly more potently compared with the CA4P group, nab-paclitaxel group and PBS group. Our results demonstrate that co-administration of CA4P increased the intratumoral accumulation of nab-paclitaxel and improved its therapeutic effect compared with single treatments.

Keywords Combination therapy · Tumor · Combretastatin A-4-phosphate · Albumin-bound paclitaxel · Tissue distribution

Introduction

Chemotherapy drugs are the basis of chemotherapy. However, adverse events caused by chemotherapy limit their clinical use. Nanocarriers have been successfully used to improve the tolerance to chemotherapy drugs due to the increased retention of the drug within the tumor from the "enhanced permeability and retention" effect [1–3]. For instance, nanoparticle albumin-bound paclitaxel (nab-paclitaxel) showed lower toxicity and higher efficacy compared with polyethylated castor oil-based paclitaxel in breast cancer treatment [4].

Despite the promising results for nanomedicines in cancer treatment, nanomedicines can generally only reach cancer cells at the edge of tumors, leaving most tumor cells in the central regions untreated due to the vascular deficiency in these central tumor regions [5–7]. Some improvement in tumor accumulation of nanomedicines has been achieved by modification of surface characteristics or size [8–10]. However, treatment with most nanomedicines still leads to concentration in the perivascular regions of the tumors.

✉ Jian Zhang
zjwonderful@hotmail.com

✉ Feng Wang
fengwangcn@hotmail.com

[1] Nanjing Medical University, Nanjing 211166, Jiangsu Province, People's Republic of China

[2] Laboratory of Translational Medicine, Jiangsu Province Hospital of Integrated Traditional Chinese and Western Medicine, Nanjing University of Chinese Medicine, Nanjing 210028, Jiangsu Province, People's Republic of China

[3] Laboratory of Translational Medicine, Jiangsu Province Academy of Traditional Chinese Medicine, No. 100, Shizi Street, Hongshan Road, Nanjing 210028, Jiangsu Province, People's Republic of China

[4] Department of Nuclear Medicine, The Affiliated Nanjing Hospital of Nanjing Medical University, No. 68, Changle Road, Nanjing 210000, Jiangsu Province, People's Republic of China

Therefore, a novel strategy that can eradicate tumor cells at both the edge and central regions of a solid tumor is required to improve the therapeutic efficacy of nanomedicines.

Combretastatin A-4-phosphate (CA4P) is a vascular disrupting agent. It is currently in phase 3 clinical trials for treatment of anaplastic thyroid carcinoma. Previous studies have shown that CA4P can selectively target endothelial cells in abnormal vessels that are abundant in tumor tissues, leading to a rapid and selective vascular shutdown and massive necrosis in the tumor core [11–13]. Some reports showed that CA4P could induce necrosis in 90–99% of tumors just 24 h after a treatment dose of 100 mg/kg [14].

Recent studies have shown that combination treatment of CA4P with therapeutic drugs may help improve drug retention. Lankester et al. found that CA4P effectively increased tumor retention of a macromolecular antibody, ^{131}I-A5B7, following CA4P-induced vessel collapse. We previously demonstrated that CA4P could improve the retention time of small molecular drugs in tumors. Therefore, we hypothesized that CA4P might increase the retention of nab-paclitaxel in tumors, thereby enhancing its antitumor efficacy. In this setting, co-administration of nab-paclitaxel and CA4P may provide a synergetic antitumor effect, in which nab-paclitaxel could kill tumor cells in the peripheral regions or tumors, while CA4P could induce extensive destruction in the interior regions.

In this study, we evaluated the biodistribution and intratumoral uptake of nab-paclitaxel and paclitaxel in tumor-bearing rats treated with ^{131}I-nab-paclitaxel alone or in combination with CA4P. We also examined the antitumor efficacy of nab-paclitaxel in combination with CA4P compared with single treatment regimens.

Materials and methods

Cell line and culture

Walker 256 (W256) rat breast carcinoma cells were obtained from ATCC. Cells were cultured in Medium 199 supplemented with 5% horse serum, 100 U/ml penicillin, and 100 mg/ml of streptomycin at 37 °C in a humidified atmosphere containing 5% CO_2.

Drug preparations

CA4P (HuaMei Technology Co., Ltd, Wuhan, China) was diluted in phosphate-buffered saline (PBS) (18.75 mg/ml). Nab-paclitaxel (Celgene Corporation, Summit) was diluted in PBS (5 mg/ml).

The iodogen-coating method was used for radioiodination of nab-paclitaxel to produce ^{131}I-nab-paclitaxel. Radioiodination was conducted by adding PBS solution of nab-paclitaxel and Na^{131}I solution (volume ratio, 5:1) into an iodogen tube. The reactions were vortexed for 3 ~ 5 min at 30 °C. Thin layer chromatography was performed to determine the radiochemical yield using 10% trichloroacetate as mobile phase. ^{131}I-nab-paclitaxel was formulated with a labeling rate of 93%.

Animals and establishment of tumor model

Sprague–Dawley rats (SD; male, 250–300 g) were obtained from the Experimental Animal Center, Jiangsu Province Academy of Traditional Chinese Medicine (Nanjing, Jiangsu, China). W256 cells (5×10^6) were inoculated subcutaneously into the right flank region of rats. Experimental protocols began when tumor diameters reached 0.8 ± 0.2 cm. Tumor growth was monitored and tumor volume was calculated as follows: tumor volume = (short dimension)^2 × (long dimension) × 1/2. W256 tumor models were successfully established in all animals, and all rats survived the anesthesia, surgery and imaging procedures. All rats were provided with food and water, and housed in a facility under an equal indoor light circle. Their health, body weight and activity level were recorded daily. Animal experimentation protocols were approved by the institutional animal care and research advisory committees.

Whole-body biodistribution of ^{131}I-nab-paclitaxel

Twelve W256 tumor-bearing rats were randomly divided into two subgroups. One group received intravenous administration of CA4P (30 mg/kg) at 2 h post-injection of ^{131}I-nab-paclitaxel (14.8 MBq/kg), and the second group received intravenous administration of ^{131}I-nab-paclitaxel (14.8 MBq/kg) and PBS. All rats were euthanized by anesthetic overdose at 24 h to evaluate the levels of ^{131}I-nab-paclitaxel in the blood, heart, lung, liver, spleen, pancreas, kidney, small intestine, skeleton, muscle and tumor.

Tissues from the two experimental groups were harvested and weighed, and the activity uptake was measured with a gamma counter (WIZARD; 2470, Perkin Elmer, NY, USA). The results were expressed as percentage of the injected dose per gram of tissues (% ID/g).

After gamma counting, tumor tissues were cut into 30 μm sections with a cryostat microtome (Shandon FSE, Thermo Fisher Scientific Co., USA). The slides were exposed to a high-performance storage phosphor screen (Super Resolution Screen, Canberra-Packard, Ontario, Canada) for 12 h. Images were scanned using a Phosphor Imager scanner (CycloneTM, Canberra-Packard) with OptiquantTM software. The sections were then stained with hematoxylin and eosin (H&E) and digitally photographed.

Intratumoral uptake of paclitaxel

Liquid chromatography coupled with tandem mass spectrometry (LC–MS/MS) was used to measure paclitaxel in the above tumor samples as previously described [15–17]. Tumor samples were collected and added to ten times the volume of methanol. After homogenizing, tissue homogenate (60 µl) was mixed with 20 µl of the internal standard docetaxel solution (50 µg/ml) and 3 ml of methyl tert-butyl ether. The mixture was vortexed for 5 min and then centrifuged (3500×*g*, 5 min). The supernatant was evaporated to dryness under a stream of nitrogen in a water bath at 35 °C. The samples were diluted and injected into the LC–MS/MS system (LC: Waters ACQUITY and MS: Waters SYNAPT).

Combination therapy protocol

Twenty-four W256 tumor-bearing rats were randomly divided into four groups ($n = 6$/group): the nab-paclitaxel + CA4P group received intravenous injection of nab-paclitaxel (60 mg/kg), followed by CA4P (30 mg/kg) 2 h later; the PBS + CA4P group received CA4P (30 mg/kg) and PBS; the nab-paclitaxel + PBS group received nab-paclitaxel (60 mg/kg) and PBS; and the PBS group only received PBS. Animals in each group received sequential intravenous injections at day 0, 6, 13 and 20. Tumor necrosis ratio was monitored using magnetic resonance imaging (MRI) before administration and after injections on day 7, 14 and 21. At day 21 after the MRI scan, animals were euthanized by anesthetic overdose. All tumors were excised and cut into 5 µm sections for immunohistochemistry and postmortem histopathology verification.

Immunohistochemical analysis

The tumors from different treatment groups were fixed in 10% v/v neutral buffered formalin, embedded in paraffin, and prepared into 5 µm-thick sections. Microvessels were stained by CD31 antibody (1:200; Abcam, Cambridge, UK) to analyze the tumor vasculature. Terminal transferase dUTP nick end labeling (TUNEL) was used to assess cellular apoptosis. Four fields were chosen to analyze the results and the apoptotic index was defined as follows: apoptotic index (%) = apoptotic cells/total tumor cells × 100.

MRI

Magnetic resonance imaging was performed with a rat coil (Chenguang Medical Technologies Co., Ltd, Shanghai, China) in a clinical 1.5T MR magnet (Echo speed; GE Co., NY, USA). The rat was gas anesthetized with 2% isoflurane in the mixture of 20% oxygen and 80% room air. Under isoflurane gas anesthesia, T1-weighted (Sequence SE, TR/TE = 550 ms/24 ms) and T2-weighted images (Sequence FSE, TR/TE = 2920 ms/88 ms) were acquired. After injection of 0.2 mmol/kg of Gd-DTPA (Bayer Schering Pharma AG, Berlin, Germany), contrast-enhanced T1-weighted (CE-T1W) images were detected.

On CE-T1 images, the central non-enhancing area was delineated to estimate tumor necrosis. Ratios of tumor necrosis were defined as the volume of necrosis over that of entire tumor, i.e., necrosis ratio = Σ (area of necrosis × slice thickness)/(area of whole tumor × slice thickness) × 100%.

Statistical analysis

Data are reported as the mean ± SD. Statistical analysis was performed with SPSS for Windows software package (version 17.0; SPSS, Chicago, IL, USA). The biodistribution data of the ^{131}I-nab-paclitaxel group and ^{131}I-nab-paclitaxel + CA4P group were compared using two-tailed independent samples *t* test. For other comparisons among groups, a one-way ANOVA was used. A *p* value of less than 0.05 was considered statistically significant.

Results

Whole-body biodistribution of ^{131}I-nab-paclitaxel and intratumor accumulation of paclitaxel in W256 tumor xenografts

To evaluate the potential effects of CA4P on paclitaxel uptake, W256 tumor-bearing rats were established and treated with ^{131}I-nab-paclitaxel alone or ^{131}I-nab-paclitaxel together with CA4P, as described in "Materials and methods". The whole-body biodistributions of ^{131}I-nab-paclitaxel in both groups are presented in Fig. 1. The radioactive accumulation of ^{131}I-nab-paclitaxel within tumor tissues was significantly higher in the ^{131}I-nab-paclitaxel + CA4P group compared with the ^{131}I-nab-paclitaxel group (0.53% ± 0.06% vs. 0.27% ± 0.04% ID/g, respectively; $p < 0.05$). No significant differences were detected in the radioactivity in non-tumor tissues between both groups ($p > 0.05$). These results indicated that CA4P could significantly increase the intratumoral uptake of ^{131}I-nab-paclitaxel without affecting the biodistribution of ^{131}I-nab-paclitaxel in healthy organs.

Representative autoradiograms and corresponding H&E staining images of tumor slices from the ^{131}I-nab-paclitaxel group and ^{131}I-nab-paclitaxel + CA4P group are presented in Fig. 2a. Tumors in the ^{131}I-nab-paclitaxel + CA4P group showed a much higher uptake of ^{131}I-nab-paclitaxel compared with tumors from the ^{131}I-nab-paclitaxel group, which is consistent with the biodistribution data. As shown in Fig. 2b, the intratumoral paclitaxel concentration in the ^{131}I-nab-paclitaxel + CA4P group was significantly higher

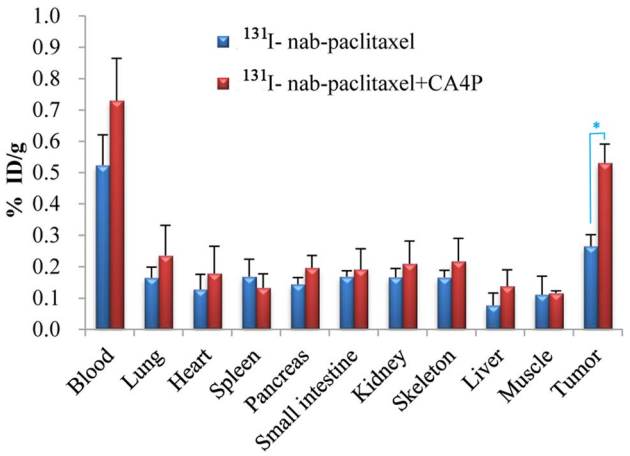

Fig. 1 Biodistribution of ^{131}I-nab-paclitaxel in W256 tumor-bearing rats treated as indicated at 24 h after administration. Data are presented as mean of %ID/g ± SD. *$p < 0.05$

than that of the ^{131}I-nab-paclitaxel group (67.45 ± 7.21 ng/ml vs. 42.37 ± 4.41 ng/ml, respectively; $p < 0.05$), which demonstrated that CA4P could increase the accumulation of paclitaxel in the tumor.

Effect of nab-paclitaxel with or without CA4P on local tumor growth

We next evaluated the effect of single treatment of either nab-paclitaxel alone or CA4P alone compared with the combination treatment of nab-paclitaxel together with CA4P on W256 tumor-bearing rats, as described in Methods. CE-T1 images revealed that all tumors at baseline (Day 0) appeared hyperenhanced (Fig. 3A1–D1), confirming abundant tumor blood supply in all model rats. After administration of nab-paclitaxel + CA4P, a thin hyperenhanced rim around the non-enhanced central region was observed (Fig. 3D2–D4). The corresponding histological results verified that the imaging changes were caused by massive central necrosis and minimum tumor residue. Tumor growth in the nab-paclitaxel + CA4P group was inhibited until the end point. In contrast, tumors in the nab-paclitaxel group exhibited more irregular enhancement (Fig. 3C4), which was confirmed by histopathology to be viable tumor tissue. Furthermore, tumors in the PBS, CA4P alone and nab-paclitaxel alone groups grew rapidly, with the tumor size progressively becoming larger.

The tumor volume growth curves in the four treatment groups are shown in Fig. 4a. No differences in tumor volumes among groups were observed at baseline ($p > 0.05$). On day 21, the nab-paclitaxel + CA4P group showed significant tumor growth inhibition compared with the other three groups ($p < 0.05$). The mean tumor volumes of the PBS, CA4P alone and nab-paclitaxel alone groups were 3.8, 2.1 and 2.7 times higher than that of the nab-paclitaxel + CA4P group, respectively. These data demonstrated that co-administration of nab-paclitaxel and CA4P exerted a stronger tumor growth inhibition effect than individual treatments.

We also examined the tumor necrosis ratio in each group from CE-T1W (Fig. 4b). Measurements at baseline were approximately 10% in all groups due to spontaneous necrosis. On day 21, a significantly increased necrosis ratio was observed in the nab-paclitaxel + CA4P group (85.78% ± 11.15%) compared with the other three groups (16.90% ± 2.10%, 26.47% ± 2.17%, and 33.57% ± 2.05% in

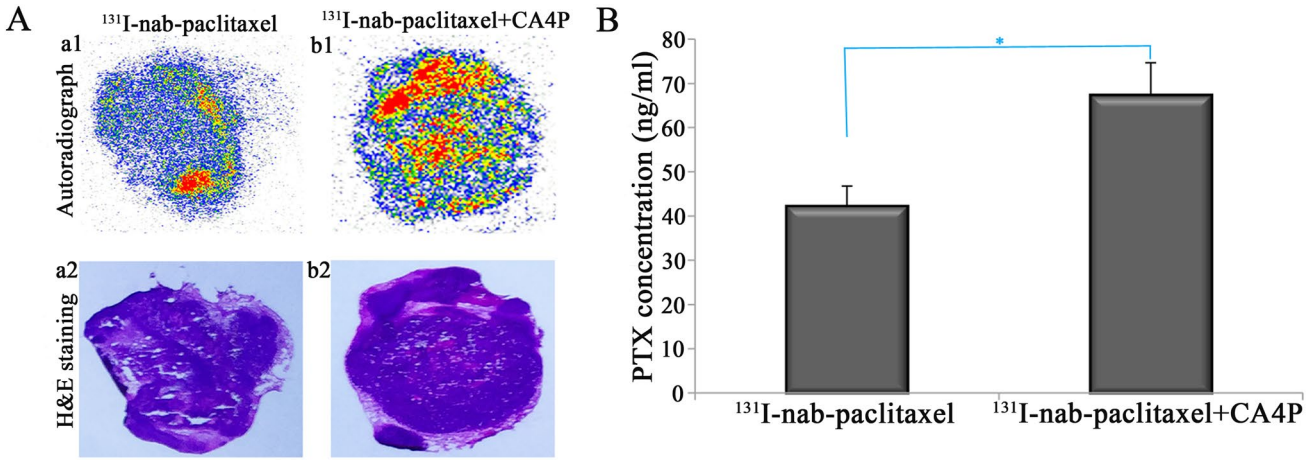

Fig. 2 Autoradiographs (a1, b1) and corresponding H&E images (a2, b2) from 30 μm tumor slices (**a**) and the intratumoral concentration of paclitaxel (**b**) at 24 h after intravenous injection of ^{131}I-nab-paclitaxel or ^{131}I-nab-paclitaxel + CA4P as indicated. From autoradiograms, the tumors in the ^{131}I-nab-paclitaxel + CA4P group revealed a much higher uptake of ^{131}I- nab-paclitaxel compared with the tumors in the ^{131}I-nab-paclitaxel group. Quantification of the intratumoral paclitaxel concentration showed that levels were significantly higher in the ^{131}I-nab-paclitaxel + CA4P group compared with the ^{131}I- nab-paclitaxel group. Data represents the mean ± SD. *$p < 0.05$

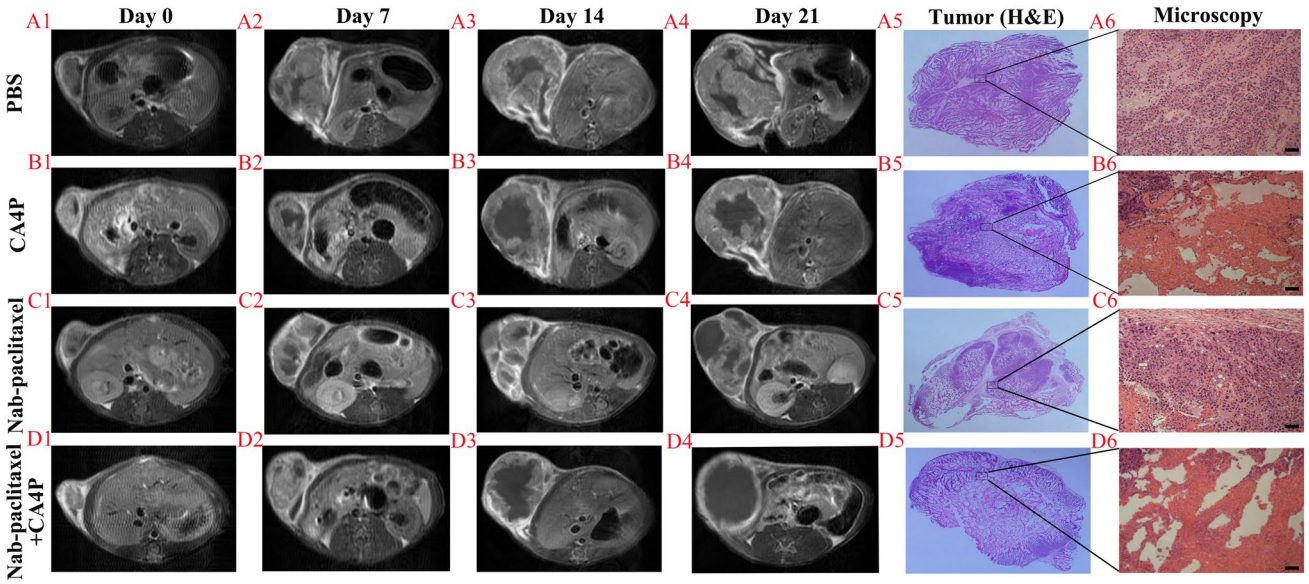

Fig. 3 CE-T1 MR imaging of the tumors from four treatment groups. Imaging shows intratumoral necrosis as well as tumor growth. At baseline (Day 0), all tumors appeared hyperenhanced. After administration of nab-paclitaxel + CA4P, a thin hyperenhanced rim surrounding the unenhanced masses was observed (D2–D4). Histological results confirm massive central necrosis and minimum tumor residue. In contrast, the tumors in the other three groups show irregular enhanced rims, and histopathology results indicate viable tumor tissues. Furthermore, tumors in the PBS, CA4P and nab-paclitaxel groups grew faster than that of the nab-paclitaxel + CA4P group. Scale bar = 50 μm

the PBS, CA4P, and nab-paclitaxel groups, respectively) ($p < 0.01$). These results further demonstrate the antitumor efficacy of co-administration of nab-paclitaxel and CA4P.

We next examined the vascular effect of treatments by performing immunohistochemistry for CD31 (Fig. 5a). The microvessel density in tumors from the nab-paclitaxel + CA4P co-treatments was lower compared with the microvessel density in tumors in the PBS, nab-paclitaxel and CA4P groups.

We also evaluated the effects of treatment on apoptosis. TUNEL staining showed that co-administration of nab-paclitaxel and CA4P significantly induced apoptosis to higher levels compared with the other treatment groups (Fig. 5b). A significantly increased apoptosis ratio was observed in the nab-paclitaxel + CA4P group (54.72% ± 3.61%) compared with the other three groups (2.53% ± 0.55%, 19.51% ± 1.74%, 33.12% ± 1.12% for the PBS, CA4P, and nab-paclitaxel groups, respectively) ($p < 0.01$) (Fig. 5c). These data further demonstrate the potent antitumor effects of co-administration of nab-paclitaxel and CA4P compared with single treatments.

Discussion

Here, we demonstrated that CA4P could improve the accumulation of nab-paclitaxel in Walker 256 carcinoma tumors and enhance the antitumor effects of nab-paclitaxel compared with administration of nab-paclitaxel or CA4P alone.

Although previous studies showed that nanocarrier-loaded paclitaxel increased intratumoral uptake of paclitaxel compared with free paclitaxel, the spatial distribution of nab-paclitaxel in untreated tumors was still heterogeneous and retained in the outer regions of tumors, where the interstitial fluid pressure was low compared with the central tumor regions [18]. The poor distribution may also result from heterogeneous blood flow together with slow interstitial diffusion [19]. In the current study, we found that addition of CA4P at 2 h after nab-paclitaxel administration resulted in an increase in nab-paclitaxel retention compared with administration of nab-paclitaxel alone. This may be mainly attributed to the trapping effect of CA4P [20], which could improve the retention of nab-paclitaxel within the tumor site, with nab-paclitaxel remaining within the tumor environment at a high concentration. Lankester et al. obtained somewhat similar results, demonstrating that CA4P effectively increased tumor retention of the macromolecular antibody ^{131}I-A5B7 following CA4P-induced vessel collapse [21].

Some researchers designed a nanocell that releases an anti-angiogenic drug from the outer shell, leading to a rapid vascular shutdown, as well as a chemotherapy drug from the inner nanoparticle that is trapped inside the tumor [22]. However, this strategy needs to strictly control the release time of the anti-angiogenesis agent, otherwise the

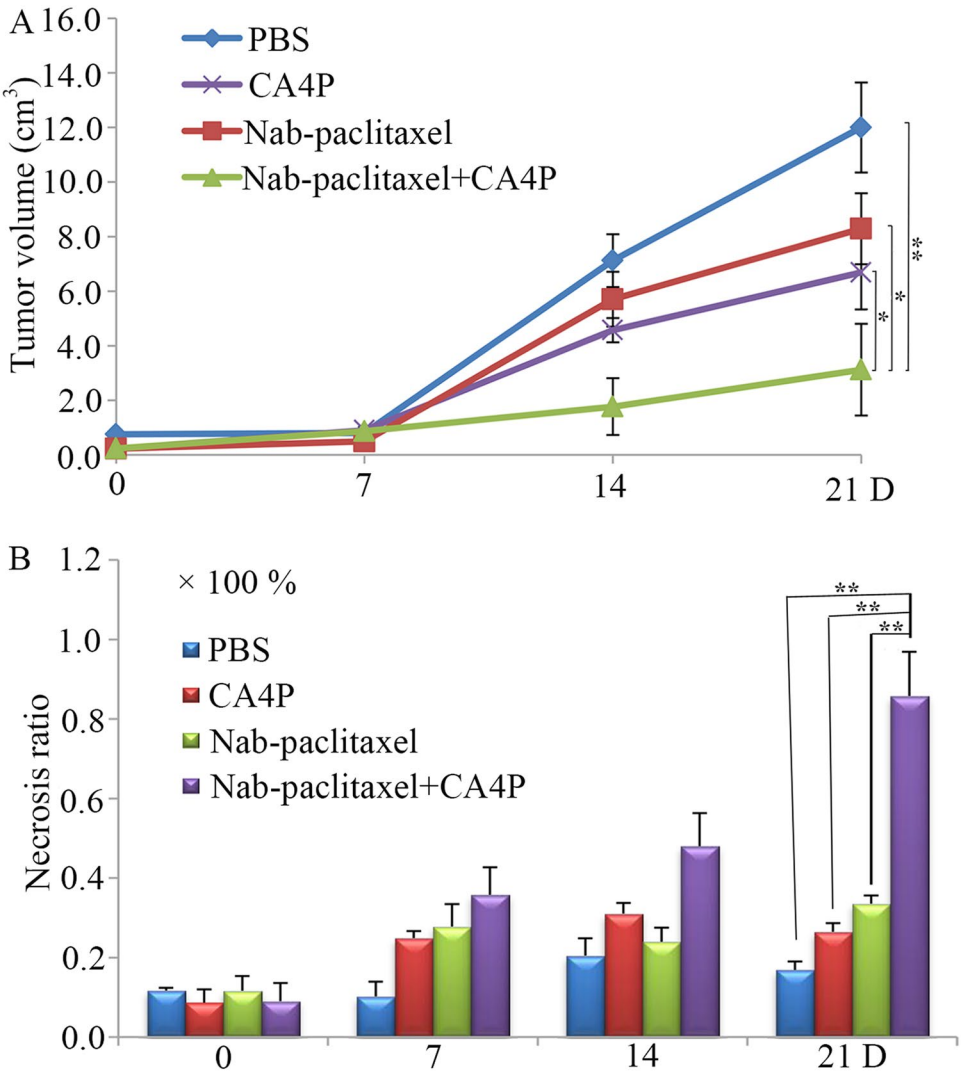

Fig. 4 Antitumor activity of different treatment groups on W256 tumor-bearing rats. **a** Tumor growth curve in the four treatment groups. No differences in tumor volumes were observed at baseline ($p > 0.05$). On day 21, the tumor volumes in the PBS, CA4P and nab-paclitaxel groups were significantly larger than that in the nab-paclitaxel + CA4P group. *$p < 0.05$, **$p < 0.01$. Tumor necrosis ratios on day 0, 7, 14 and 21 post-treatment in the four treatment groups. **b** Tumor necrosis ratio measured from CE-T1W was about 10% in each group at baseline because of spontaneous necrosis. On day 21, a significantly higher necrosis ratio was observed in the nab-paclitaxel + CA4P group compared with the PBS, CA4P and nab-paclitaxel groups. **$p < 0.01$

early release of anti-angiogenesis agent would induce vascular collapse preventing subsequent nanodrug entry. In comparison, administration of the combination of nanodrug and CA4P is easy to control drug release. After loading the tracer on the nanodrug, the release time of CA4P can be precisely controlled under the guidance of molecular images.

This combination treatment strategy can be used to reduce toxic side effects in breast cancer patients by allowing a reduction of systemic doses of nab-paclitaxel or other cytotoxic drugs. Nab-paclitaxel is currently used in the clinic, and CA4P is under phase III clinical trials. The combination of these two drugs may be applied to the suitable cancer patients when CA4P enters clinical use.

Researchers have made some efforts to improve the uptake of nanodrugs within tumors. In these strategies, cytotoxic drugs (docetaxel, doxorubicin) are used to induce apoptosis to improve nanomedicine accumulation in the tumor [23]. Nonetheless, these strategies show some limitations, as the cytotoxic drugs also induce toxicity to normal tissues and lack tumor specificity [24, 25].

Our results showed that the tumor volumes in the nab-paclitaxel and CA4P group were smaller than that of the other treatment groups. Moreover, the tumor apoptosis ratio and necrosis ratio were higher in the nab-paclitaxel + CA4P group compared with the single treatment groups. These data indicate that the co-administration of nab-paclitaxel and CA4P produced stronger tumor growth inhibition. The superior efficacy of the nab-paclitaxel/CA4P combination therapy might be explained by the following mechanisms. First, CA4P may trap nab-paclitaxel within the tumor following CA4P-induced vessel collapse, resulting in increased retention of nab-paclitaxel within the tumor site. The other advantage of combining nab-paclitaxel with CA4P is the multi-targeting strategy, as nab-paclitaxel acts on the proliferating tumor cells at the tumor periphery, while CA4P targets endothelial cells and induces necrosis at the center of the tumor.

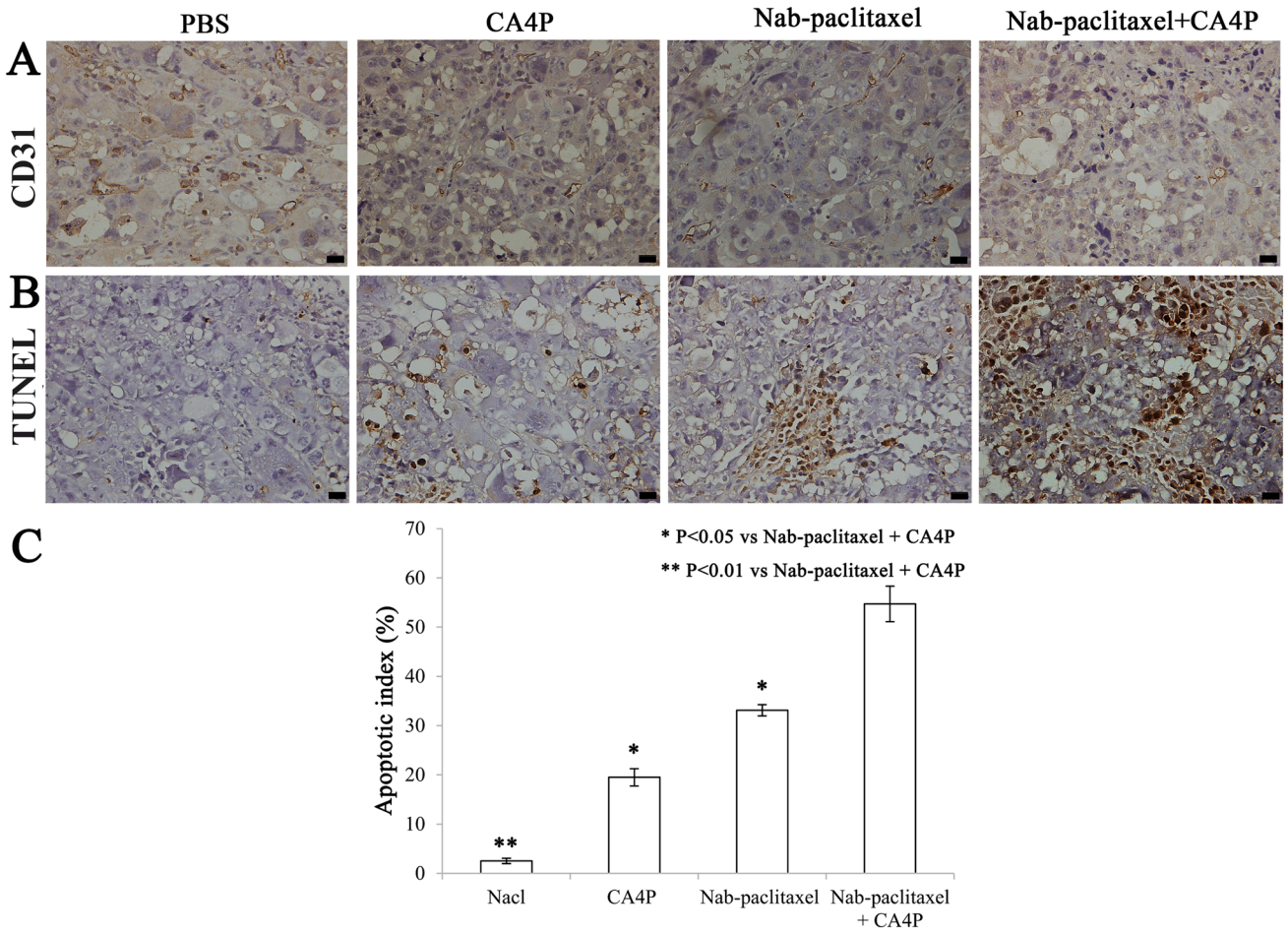

Fig. 5 Effect of different treatment groups on tumor microvessels and cell apoptosis in vivo. **a** Immunostaining with anti-CD31 was used to detect tumor vasculature. **b** Cellular apoptosis was determined by TUNEL assay. **c** The apoptotic index was calculated as a ratio of the apoptotic cell number to the total cell number in each field. Data represent the mean ± SD

This study has some limitations. The 2 h interval used in our research was based on the onset time of CA4P on tumor vessels in our pre-experiment carried out with nab-paclitaxel in combination with CA4P. We also did not compare treatment outcomes in response to nab-paclitaxel and CA4P administration at different intervals. Nonetheless, our findings provide preliminary data demonstrating that inclusion of CA4P with nab-paclitaxel treatment against breast carcinoma could improve the therapeutic effects of nab-paclitaxel and show great promise for the combination strategy in clinics. In addition, another limitation in the experiment is the use of only one animal model, the Walker 256 in rats. A follow-up study will explore the related issues.

Acknowledgements We thank Edanz Group (http://www.edanzediting.com/ac) for editing a draft of this manuscript.

Funding This work was supported by the National Natural Science Foundation of China (No. 81473120).

Compliance with ethical standards

Conflict of interest The authors declare no potential conflict of interests.

Ethics approval All animal experiments were carried out in accordance with international ethical guidelines and the National Institutes of Health Guide concerning the Care and Use of Laboratory Animals. The animal experiments were approved by the Experimental Animal Ethics Committee Jiangsu Provincial Institute of Traditional Chinese Medicine.

References

1. Matsumura Y, Maeda H (1986) A new concept for macromolecular therapeutics in cancer chemotherapy: mechanism of tumoritropic accumulation of proteins and the antitumor agent smancs. Cancer Res 46:6387–6392
2. Maeda H, Nakamura H, Fang J (2013) The EPR effect for macromolecular drug delivery to solid tumors: improvement of tumor

uptake, lowering of systemic toxicity, and distinct tumor imaging in vivo ☆. Adv Drug Deliv Rev 65:71–79
3. Moon JH Jr, Moxley J, Zhang P, Cui H (2015) Nanoparticle approaches to combating drug resistance. Future Med Chem 7:1503
4. Petrelli F, Borgonovo K, Barni S (2010) Targeted delivery for breast cancer therapy: the history of nanoparticle-albumin-bound paclitaxel. Expert Opin Pharmacother 11:1413
5. Sykes EA, Chen J, Zheng G, Chan WC (2014) Investigating the impact of nanoparticle size on active and passive tumor targeting efficiency. ACS Nano 8:5696–5706
6. Yuan F, Leunig M, Huang SK, Berk DA, Papahadjopoulos D, Jain RK (1994) Microvascular permeability and interstitial penetration of sterically stabilized (stealth) liposomes in a human tumor xenograft. Cancer Res 54:3352–3356
7. Kobayashi H, Watanabe R, Choyke PL (2013) Improving conventional enhanced permeability and retention (EPR) effects; What is the appropriate target? Theranostics 4:81–89
8. Riché EL, Erickson BW, Cho MJ (2004) Novel long-circulating liposomes containing peptide library-lipid conjugates: synthesis and in vivo behavior. J Drug Target 12:355
9. Cukierman E, Khan DR (2010) The benefits and challenges associated with the use of drug delivery systems in cancer therapy. Biochem Pharmacol 80:762–770
10. Liechty WB, Peppas NA (2012) Expert opinion: responsive polymer nanoparticles in cancer therapy. Eur J Pharm Biopharm Official J Arbeitsgemeinschaft Fur Pharmazeutische Verfahrenstechnik E V 80:241
11. Dark GG, Hill SA, Prise VE, Tozer GM, Pettit GR, Chaplin DJ (1997) Combretastatin A-4, an agent that displays potent and selective toxicity toward tumor vasculature. Cancer Res 57:1829
12. Vincent L, Kermani P, Young LM et al (2005) Combretastatin A4 phosphate induces rapid regression of tumor neovessels and growth through interference with vascular endothelial-cadherin signaling. J Clin Investig 115:2992–3006
13. Siemann DW, Chaplin DJ, Horsman MR (2004) Vascular-targeting therapies for treatment of malignant disease. Cancer 100:2491–2499
14. Chaplin DJ, Pettit GR, Hill SA (1999) Anti-vascular approaches to solid tumour therapy: evaluation of combretastatin A4 phosphate. Anticancer Res 19:189
15. Parise RA, Ramanathan RK, Zamboni WC, Egorin MJ (2003) Sensitive liquid chromatography-mass spectrometry assay for quantitation of docetaxel and paclitaxel in human plasma. J Chromatogr B 783:231–236
16. Tong X, Zhou J, Tan Y (2006) Liquid chromatography/tandem triple-quadrupole mass spectrometry for determination of paclitaxel in rat tissues. Rapid Commun Mass Spectrom Rcm 20:1905–1912
17. Gallo JM, Li S, Guo P, Reed K, Ma J (2003) The effect of P-glycoprotein on paclitaxel brain and brain tumor distribution in mice. Cancer Res 63:5114
18. Eikenes L, Bruland ØS, Brekken C, Davies CL (2004) Collagenase increases the transcapillary pressure gradient and improves the uptake and distribution of monoclonal antibodies in human osteosarcoma xenografts. Cancer Res 64:4768–4773
19. Jain RK, Stylianopoulos T (2010) Delivering nanomedicine to solid tumors. Nat Rev Clin Oncol 7:653
20. Gao M, Yao N, Huang D et al (2015) Trapping effect on a small molecular drug with vascular-disrupting agent CA4P in rodent H22 hepatic tumor model: in vivo magnetic resonance imaging and postmortem inductively coupled plasma atomic emission spectroscopy. J Drug Target 23:436
21. Lankester KJ, Maxwell RJ, Pedley RB et al (2007) Combretastatin A-4-phosphate effectively increases tumor retention of the therapeutic antibody, 131I-A5B7, even at doses that are sub-optimal for vascular shut-down. Int J Oncol 30:453–460
22. Sengupta S, Eavarone D, Capila I et al (2005) Temporal targeting of tumour cells and neovasculature with a nanoscale delivery system. Nature 436:568–572
23. Griffon-Etienne G, Boucher Y, Brekken C, Suit HD, Jain RK (1999) Taxane-induced apoptosis decompresses blood vessels and lowers interstitial fluid pressure in solid tumors: clinical implications. Cancer Res 59:3776–3782
24. Li Y, Wang J, Wientjes MG, Au JLS (2012) Delivery of nanomedicines to extracellular and intracellular compartments of a solid tumor. Adv Drug Deliv Rev 64:29–39
25. Feng SS, Shu C (2003) Chemotherapeutic engineering: application and further development of chemical engineering principles for chemotherapy of cancer and other diseases. Chem Eng Sci 58:4087–4114